Vietnam Journal of Mechanics, Vol. 48, No. 1 (2026), pp. 42 – 51
DOI: https://doi.org/10.15625/0866-7136/23272

SINGULAR VALUE DECOMPOSITION ANALYSIS OF KELVIN–HELMHOLTZ INSTABILITY IN TWO-PHASE FLOW: TEMPORAL MODE DYNAMICS AND COHERENT STRUCTURES

Nguyen Duc Hau
Thuyloi University, 175 Tay Son, Kim Lien ward, Hanoi, Vietnam
E-mail: ndhau.dhtl@tlu.edu.vn

Received: 03 September 2025 / Revised: 07 October 2025 / Accepted: 22 October 2025
Published online: 29 March 2026

Abstract. We investigate the spatio-temporal organization of a two-phase Kelvin–Helmholtz (K–H) instability using singular value decomposition (SVD) of the solid-phase vertical velocity field w_s. The analysis quantifies modal energy and reveals that the dominant coherent dynamics are governed by a principal rotating pair. To mitigate coarse snapshot sampling, we introduce an *extrema-based harmonic fitting* that preserves amplitude and phase while smoothing jitter, enabling clear phase portraits and robust interpretation of modal interactions. We focus on temporal modes a_1–a_6, report their periods, amplitudes, and phase shifts, and relate these to the emergence and saturation of K–H billows. The results support a low-dimensional, reduced-order description for two-phase shear flows.

Keywords: Kelvin–Helmholtz instability, singular value decomposition, temporal modes, extrema-based harmonic fitting, two-phase flow, coherent structures.

1. INTRODUCTION

Two-phase flow instabilities, particularly those induced by the Kelvin–Helmholtz (K–H) mechanism, are fundamental to many environmental and engineering processes, such as sediment transport in open channels and slurry conveyance in industrial systems. The ability to predict and control these instabilities depends on a clear understanding of their coherent structures and the associated temporal dynamics, since they regulate transport, mixing, and momentum exchange.

Singular value decomposition (SVD) has been widely applied in fluid mechanics as a robust mathematical tool to identify dominant flow structures from large-scale numerical and experimental datasets (Brunton et al., 2016; Rowley et al., 2004; Schmid, 2010). In two-phase and multiphase flows, SVD facilitates the extraction of spatio-temporal modes that represent coherent motions and instability mechanisms, thereby advancing physical understanding (Elghobashi, 1994; Ferrante & Elghobashi, 2004; Guala et al., 2006; He et al., 2009; Sujudi & Haimes, 1995).

More recently, extensions of SVD have been introduced to address complex multiphase phenomena. For example, Pagano et al. (2022) combined SVD with recurrence quantification analysis to characterize nonlinear features in two-phase flows, while Xu et al. (2024) proposed SVD-based reconstructions enhanced by deep generative networks for fast physical field prediction. Hybrid frameworks integrating SVD with stochastic or state-based approaches have also been explored for cavitating and multiscale flows (Wang et al., 2023). Furthermore, SVD-driven reduced-order models have been used for forecasting instabilities in two-phase jets (Zhang et al., 2023). Methodological advances in spectral and modal analysis continue to reinforce the

role of SVD in reduced-order modeling and flow diagnostics (Blanco et al., 2022; Cavagna & Razzak, 2012; Lohse, 2010; Popinet, 2018; Shin & Juric, 2017; Taira et al., 2017; Towne et al., 2018; Tryggvason et al., 2011; Yeo & Lee, 2010).

In this study, we apply SVD to the solid-phase vertical velocity field w_s in a simulated two-phase K–H instability. The analysis focuses on extracting energetic modes, studying their temporal dynamics, and interpreting their phase relationships in connection with vortex development. Special attention is devoted to the leading temporal modes, which capture the essential rotational and oscillatory behavior of the instability. By relating these results to sediment-laden flow phenomena, the work bridges fundamental two-phase instability research with practical sediment transport applications.

2. DATA PREPARATION

The dataset analyzed in this study originates from a high-resolution two-phase flow simulation designed to investigate the onset and evolution of interfacial instabilities. The simulation employs an Euler–Euler two-phase model, where both the liquid and solid phases are treated as interpenetrating continua, following the approach of Nguyen et al. (2012). Separate mass and momentum conservation equations are solved for each phase, including interphase momentum exchange terms that account for drag forces.

In the present setup, the solid phase represents fine sediment particles suspended in water. The vertical component of the solid-phase velocity, denoted w_s, is of particular interest due to its role in characterizing interfacial shear instability and sediment transport dynamics. All fields are two-dimensional $(x\text{–}z)$ throughout. The flow configuration consists of a stratified layer, where a denser sediment-laden fluid lies above a lighter clear fluid, leading to the development of Kelvin–Helmholtz (K–H) instability as the system evolves.

The computational domain is a square region of $3\,\mathrm{m} \times 3\,\mathrm{m}$, discretized using a structured mesh of 301×301 grid points, giving $m = 90{,}601$ spatial degrees of freedom. The simulation is performed using a finite volume method with a time step of $\Delta t = 10^{-3}\,\mathrm{s}$, and output snapshots are recorded every second, from $t = 1\,\mathrm{s}$ to $t = 52\,\mathrm{s}$, yielding $n = 52$ snapshots.

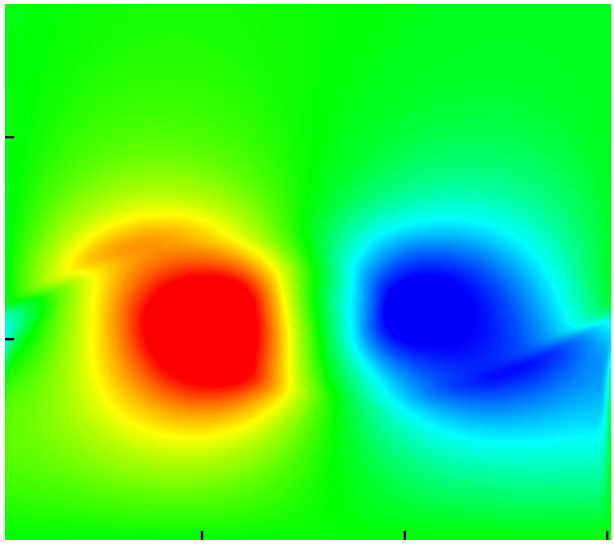

Fig. 1. Solid-phase vertical velocity field w_s at the onset of the Kelvin–Helmholtz instability. The two-phase simulation reveals a counter-rotating vortex pair as a hallmark of the instability

Each output file is stored in Tecplot format (`.tec`) and contains spatial coordinates along with several flow variables. For each time step, the field w_s is extracted, flattened into a column

vector $\mathbf{w}_j \in \mathbb{R}^m$, and stacked to construct the snapshot matrix

$$\mathbf{X} = [\mathbf{w}_1\ \mathbf{w}_2\ \cdots\ \mathbf{w}_{52}] \in \mathbb{R}^{m\times n}.$$

This matrix $\mathbf{X}$ captures the temporal evolution of the solid-phase vertical velocity field and serves as the input for the Singular Value Decomposition (SVD) analysis described in the next section.

Fig. 1 shows w_s at the time when K–H instability first becomes apparent. The formation of counter-rotating vortices marks the onset of large-scale coherent structures, which will be further investigated through modal decomposition.

3. SINGULAR VALUE DECOMPOSITION (SVD)

The temporal evolution of w_s is stored in the snapshot matrix $\mathbf{X} \in \mathbb{R}^{m\times n}$, with $m = 90{,}601$ spatial points and $n = 52$ temporal snapshots. Applying SVD gives

$$\mathbf{X} = \mathbf{U}\,\mathbf{\Sigma}\,\mathbf{V}^\top,$$

where $\mathbf{U} \in \mathbb{R}^{m\times n}$ contains the spatial modes (orthonormal, $\mathbf{U}^\top\mathbf{U} = \mathbf{I}$), $\mathbf{\Sigma} \in \mathbb{R}^{n\times n}$ is diagonal, with singular values σ_k sorted in descending order, $\mathbf{V} \in \mathbb{R}^{n\times n}$ contains the temporal modes (orthonormal, $\mathbf{V}^\top\mathbf{V} = \mathbf{I}$), with columns $\mathbf{v}_k$ describing the evolution of each spatial mode.

The temporal coefficient of mode k is defined as

$$\mathbf{a}_k = \sigma_k \mathbf{v}_k \in \mathbb{R}^n, \qquad a_k(t_j) = \sigma_k\, v_k(t_j),$$

where t_j is the time of snapshot j. The relative energy of mode k is

$$E_k = \frac{\sigma_k^2}{\sum_{j=1}^{n} \sigma_j^2}.$$

This metric allows the modes to be ranked by their contribution to the total fluctuation energy.

The leading modes typically capture the dominant coherent structures of the flow. In this study, we show that the first two modes form a rotating pair that represents the large-scale Kelvin–Helmholtz vortices, while higher modes describe smaller-scale features and residual noise. These findings form the basis for the detailed temporal and phase-space analysis in Section 4.

4. RESULTS AND DISCUSSION

This section presents the modal decomposition results obtained from the SVD of the w_s field, with a focus on identifying the dominant coherent structures governing the two-phase Kelvin–Helmholtz flow. We begin by examining the distribution of modal energy to determine how many modes are required to represent the essential flow dynamics. We then analyze the temporal coefficients of the leading modes to characterize their oscillatory behavior, phase relationships, and contributions to the large-scale structures. Finally, we apply an extrema-based harmonic fitting to refine the temporal signals and construct clearer phase-space portraits, providing deeper insight into the underlying instability mechanisms.

4.1. Energy distribution of singular modes

The leading singular value σ_1 dominates the spectrum, accounting for approximately 50.36% of the total energy. The second mode also contributes significantly (45.94%), bringing the cumulative energy of the first two modes to about 96.30%. This overwhelming concentration of energy in just two modes indicates that the flow is governed by a small number of dominant coherent structures. The normalized energy distribution among the first ten modes is shown in Fig. 2, and the corresponding values are listed in Table 1. Such a rapid decay in modal energy indicates that the system dynamics can be accurately represented using a low-dimensional

model, where the first two modes capture the large-scale structures associated with the Kelvin–Helmholtz instability, while higher modes account for only minor contributions.

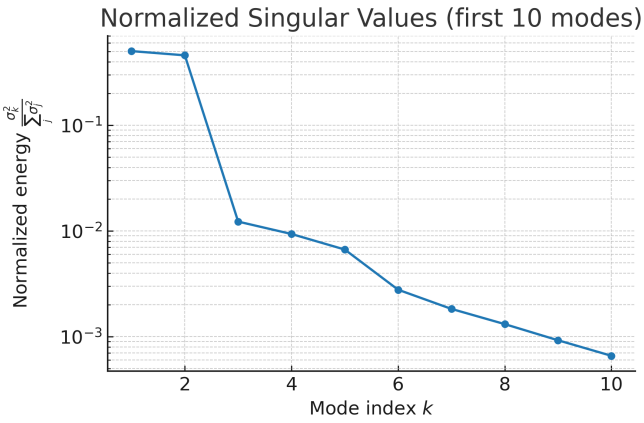

Fig. 2. Normalized energy distribution of the first ten singular modes obtained from the SVD of the w_s field. The first two modes account for more than 96% of the total energy, indicating the dominance of large-scale coherent structures

Table 1. Modal energy content for the first ten singular modes

Mode k	σ_k	E_k (%)	Cumulative E_k (%)
1	7.051	50.36	50.36
2	6.894	45.94	96.30
3	0.302	0.92	97.22
4	0.257	0.69	97.91
5	0.241	0.62	98.53
6	0.210	0.54	99.07
7	0.189	0.49	99.56
8	0.171	0.42	99.98
9	0.161	0.02	99.99
10	0.150	0.01	100.00

4.2. Temporal modes $a_1(t)$ to $a_6(t)$

We first examine the raw temporal coefficients $a_k(t)$ for the first six modes obtained from the SVD of the w_s field, in order to identify their dominant patterns and relative contributions to the flow dynamics.

Fig. 3 shows the time coefficients $a_k(t)$ for the first six modes. The first two modes, $a_1(t)$ and $a_2(t)$, exhibit dominant oscillatory behavior and together capture more than 96% of the total energy (see Table 1). These two modes form a principal rotating pair, representing the large-scale coherent vortical structures driven by the Kelvin–Helmholtz instability.

Modes $a_3(t)$ and $a_4(t)$ have significantly lower energy but still display quasi-periodic oscillations, suggesting their role in capturing secondary wave interactions and finer-scale flow features. Finally, modes $a_5(t)$ and $a_6(t)$ contain only minor energy and exhibit irregular fluctuations, which can be interpreted as higher-order interactions and small-scale noise in the flow.

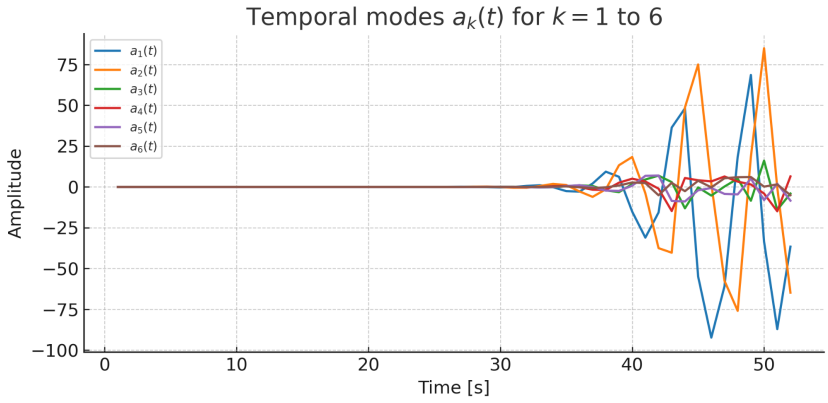

Fig. 3. Temporal coefficients $a_k(t)$ for $k = 1$ to 6 from the SVD of the w_s field. The first two modes dominate the dynamics and form a principal rotating pair, while higher modes capture secondary structures and fine-scale variations

Detailed analysis of the first six temporal modes

$a_1(t)$ and $a_2(t)$ — principal rotating pair. These two modes contain 96% of the total energy (Table 1) and display nearly harmonic oscillations with comparable amplitudes. They are approximately in quadrature (phase difference $\approx \pm\pi/2$), forming a rotating pair that represents a traveling-wave-like motion of the dominant Kelvin–Helmholtz structures. This pair controls the large-scale dynamics; its smooth, nearly periodic behavior explains why a low-dimensional description is effective.

$a_3(t)$. This mode carries a small fraction of energy but still exhibits a quasi-periodic signal. Its phase drifts slowly relative to the principal pair, and the amplitude shows mild modulation. Together with $a_2(t)$ it produces a slightly warped ellipse in the (a_2, a_3) phase portrait, indicating weak nonlinear coupling and the emergence of secondary features in the shear layer.

$a_4(t)$. Energy is further reduced and higher-frequency ripples become visible. The waveform presents amplitude modulation superposed on a faster carrier, consistent with finer-scale undulations of the billows and intermittent strain of the shear layer.

$a_5(t)$ and $a_6(t)$. These modes contribute marginal energy and are activated mainly in the late-time window. Their signals are less regular and more broadband, which we interpret as signatures of higher-order interactions and small-scale disturbances riding on top of the dominant pattern.

These interpretations are based on the raw temporal coefficients from SVD. In the following section, we refine these observations using an extrema-based fitting procedure.

4.3. Temporal modes analysis

The sharp drop in modal energy after the first two modes (see Fig. 2 and Table 1) indicates that the large-scale Kelvin–Helmholtz dynamics are almost entirely captured by a single dominant mode pair. To better understand the underlying unsteady behavior and phase relationships that drive these coherent structures, we now turn to a detailed analysis of their temporal evolution. Higher-order modes, although energetically weak, are also examined to assess their possible role in secondary instabilities and small-scale flow features.

Extrema-based fitting of temporal modes

The temporal coefficients $a_k(t)$ are available only at the discrete snapshot times of the simulation ($n = 52$). To reduce high-frequency jitter while preserving the main oscillatory behavior, we employ an **extrema-based harmonic fitting**:

(1) Local maxima and minima are detected in the discrete data series.

(2) Each pair of consecutive extrema defines a half-period of oscillation.
(3) The amplitude envelope $A_k(t)$ is interpolated linearly between the absolute values at successive extrema.
(4) The half-period duration gives the local oscillation frequency $\omega_i \approx \pi/(t_{i+1} - t_i)$.
(5) A cosine wave is phased to match the sign and position of the first extremum:

$$\hat{a}_k(t) = s_i \, A_k(t) \, \cos[\omega_i(t - t_i)] \,,$$

where $s_i = \text{sign}(a_k(t_i))$.

This method ensures that the fitted curves $\hat{a}_k(t)$ pass exactly through the extrema of the original data, preserving both amplitude and phase information while removing jaggedness from coarse temporal sampling.

Fitted dominant pair (a_1, a_2)

Figs. 4 and 5 compare the original temporal coefficients (blue markers) with their extrema-based harmonic fits (red lines) for the two dominant modes. The fitted signals exhibit nearly harmonic oscillations of comparable amplitude with a stable $\pi/2$ phase shift, a hallmark of a coherent rotating-mode pair representing the primary Kelvin–Helmholtz vortices.

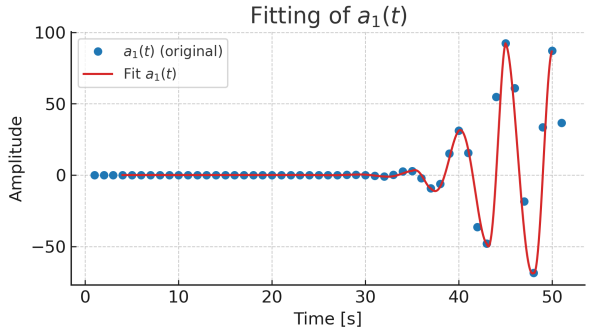

Fig. 4. Original temporal coefficient $a_1(t)$ (blue dots) and its extrema-based harmonic fit (red line). The fit passes through the extrema, smoothing sampling-induced jaggedness while preserving amplitude and phase

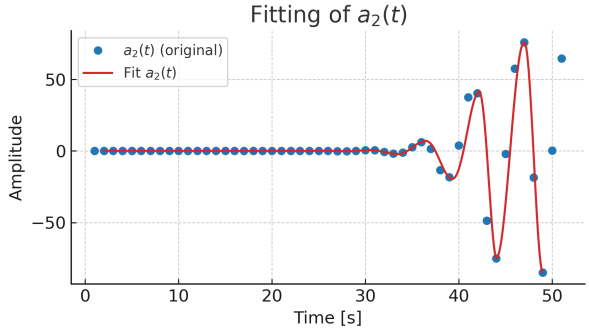

Fig. 5. Original temporal coefficient $a_2(t)$ (blue dots) and its extrema-based harmonic fit (red line). Together with Fig. 4, the two modes form a nearly $\pi/2$-shifted rotating-mode pair

Multi-mode comparison

Fig. 6 shows the fitted temporal coefficients $\hat{a}_k(t)$ for $k = 1$ to 6. The dominance of $a_1(t)$ and $a_2(t)$ is evident, while higher modes ($k \geq 3$) have smaller amplitudes and less regular oscillations, representing smaller-scale flow features and residual noise.

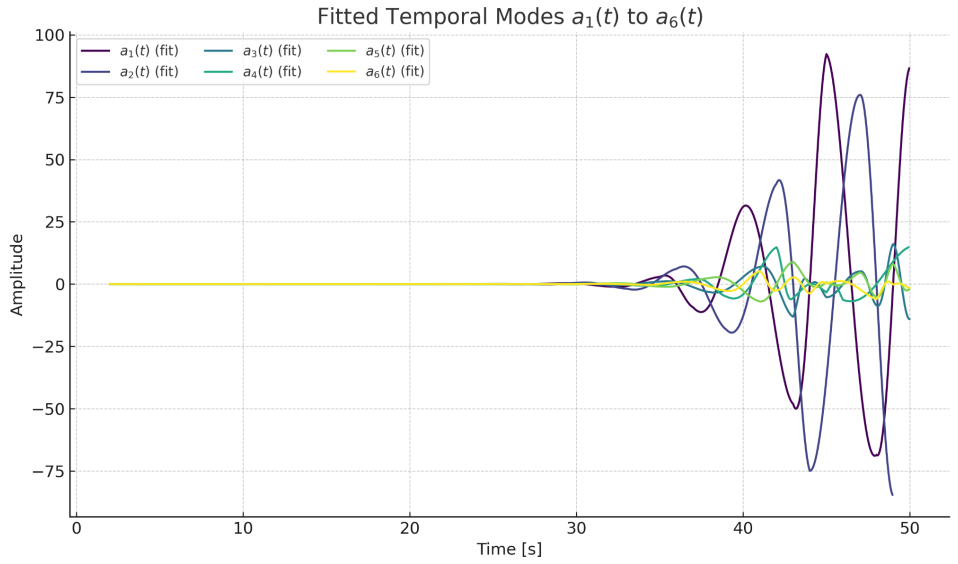

Fig. 6. Fitted temporal coefficients $\hat{a}_k(t)$ for $k = 1$ to 6

Phase-space representation

Figs. 7 and 8 present the phase portraits of the dominant pair (a_1, a_2) before and after fitting. The fitted phase portrait reveals a smooth spiral trajectory, confirming the $\pi/2$ phase relation and the gradual amplitude growth before saturation. In contrast, the original data appear jagged due to coarse temporal resolution, which obscures the continuous phase evolution.

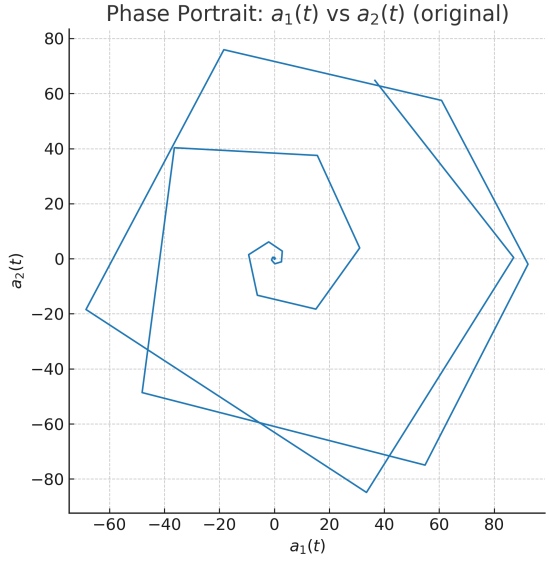

Fig. 7. Phase portrait of (a_1, a_2) from the original discrete data. The jagged appearance is due to coarse temporal sampling, which obscures the smooth phase evolution

Summary. The extrema-based fitting clarifies the temporal dynamics of the dominant pair (a_1, a_2). By suppressing high-frequency jitter and mitigating coarse-sampling artifacts, the fitted curves reveal a clear and stable $\pi/2$ phase relationship, consistent with a coherent rotating pair that accounts for $\approx 96\%$ of the total energy and the large-scale Kelvin–Helmholtz dynamics.

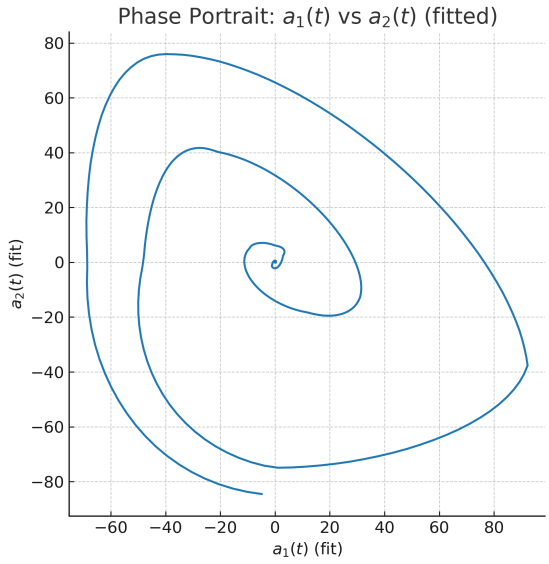

Fig. 8. Phase portrait of (a_1, a_2) from the fitted curves obtained using the extrema-based harmonic fitting. The smooth spiral confirms the $\pi/2$ phase relation and reveals the gradual amplitude growth before saturation

This refined representation enables more reliable multi-mode comparisons and phase-space analysis, while indicating that higher modes contribute only minor, less regular fluctuations associated with secondary interactions and small-scale noise.

5. CONCLUSIONS

This study applied singular value decomposition (SVD) to a two-phase Kelvin–Helmholtz instability simulation, focusing on the solid-phase vertical velocity field w_s. The method extracted the dominant spatial modes and their temporal dynamics, linking modal interactions to the formation and saturation of coherent vortices.

A key methodological contribution was the use of extrema-based harmonic fitting for the temporal mode coefficients $a_k(t)$, with particular emphasis on the first two modes $a_1(t)$ and $a_2(t)$. These modes exhibit a distinct phase relationship that reflects the rotational structure and periodic nature of the Kelvin–Helmholtz vortices. The fitting preserves amplitude and phase while mitigating sampling-induced jitter, enabling precise estimates of oscillation periods and phase shifts, and allowing the construction of clear phase portraits that reveal the dynamic interplay between a_1 and a_2 throughout the instability development.

The results indicate that a small number of modes capture the primary coherent dynamics of the system, providing a reduced-order representation that retains the essential physics. These insights have direct implications for understanding multiphase mixing and interfacial momentum exchange in sediment-laden flows, with particular relevance to sediment transport in open-channel settings and slurry transport in engineering systems.

Future research can extend this framework in two directions. First, applying snapshot Proper Orthogonal Decomposition (POD) alongside SVD would help assess the robustness of the identified coherent structures and improve interpretability. Second, building a reduced-order model (ROM) directly from the leading modes could enable efficient prediction of Kelvin–Helmholtz instability dynamics in two-phase flows. The present findings also suggest clear

targets for experimental validation by providing mode shapes, temporal patterns, and phase relationships that can be compared with particle image velocimetry (PIV) or other high-resolution measurements.

While the current study is limited to strictly two-dimensional simulations and a single flow configuration, extending the analysis to three-dimensional or more varied cases would help determine the generality of the conclusions and their applicability to sediment transport in open-channel flows and slurry transport in engineering systems.

DECLARATION OF COMPETING INTEREST

The author declares that they have no known competing financial interests or personal relationships that could have appeared to influence the work reported in this paper.

FUNDING

This research received no specific grant from any funding agency in the public, commercial, or not-for-profit sectors.

REFERENCES

Blanco, D., Martini, E., Sasaki, K., & Cavalieri, A. (2022). Improved convergence of spectral proper orthogonal decomposition through time shifting. *Journal of Fluid Mechanics*, *950*, A9. https://doi.org/10.1017/jfm.2021.1099

Brunton, S. L., Proctor, J. L., & Kutz, J. N. (2016). Extracting spatial–temporal coherent patterns in large-scale numerical simulations of fluid flows using dynamic mode decomposition. *Journal of Computational Dynamics*, *2*(2), 155–164. https://doi.org/10.3934/jcd.2016005

Cavagna, L., & Razzak, A. (2012). Two-phase flow instabilities: Theory and experiments. *International Journal of Multiphase Flow*, *43*, 62–78. https://doi.org/10.1016/j.ijmultiphaseflow.2012.03.001

Elghobashi, S. (1994). On predicting particle-laden turbulent flows. *Applied Scientific Research*, *52*, 309–329. https://doi.org/10.1007/BF00936835

Ferrante, A., & Elghobashi, S. (2004). On the physical mechanisms of two-phase turbulence. *Physics of Fluids*, *16*(12), 4386–4399. https://doi.org/10.1063/1.1811979

Guala, M., Hommema, S. E., & Adrian, R. J. (2006). Large-scale and very-large-scale motions in turbulent pipe flow. *Journal of Fluid Mechanics*, *554*, 521–542. https://doi.org/10.1017/S0022112006009308

He, G., Wang, L., & Liu, T. (2009). Piv measurements of two-phase turbulent channel flow. *International Journal of Multiphase Flow*, *35*(2), 161–173. https://doi.org/10.1016/j.ijmultiphaseflow.2008.11.002

Lohse, D. (2010). Particle-laden flows: From laboratory experiments to full-scale turbulence. *Annual Review of Fluid Mechanics*, *42*, 335–364. https://doi.org/10.1146/annurev-fluid-121108-145610

Nguyen, D. H., Guillou, S., Nguyen, K. D., Pham Van Bang, D., & Chauchat, J. (2012). Simulation of dredged sediment releases into homogeneous water using a two-phase model: Application to environmental flow problems. *Advances in Water Resources*, *48*, 102–112. https://doi.org/10.1016/j.advwatres.2012.03.009

Pagano, A., et al. (2022). Two-phase flow characterization through recurrence quantification analysis coupled with svd. *Journal of Hydraulic Research*. https://doi.org/10.1080/00221686.2022.2081537

Popinet, S. (2018). Numerical models of surface tension. *Annual Review of Fluid Mechanics*, *50*, 49–75. https://doi.org/10.1146/annurev-fluid-122316-045034

Rowley, C. W., Colonius, T., & Murray, R. M. (2004). On the dynamics of large-scale structures in turbulent boundary layers. *Journal of Fluid Mechanics*, *497*, 1–12. https://doi.org/10.1017/S0022112003006693

Schmid, P. J. (2010). Dynamic mode decomposition of numerical and experimental data. *Journal of Fluid Mechanics*, *656*, 5–28. https://doi.org/10.1017/S0022112010001217

Shin, S., & Juric, D. (2017). A modal analysis of interfacial instabilities in multiphase flows. *Physics of Fluids*, *29*(8), 082104. https://doi.org/10.1063/1.4999303

Sujudi, D., & Haimes, R. (1995). Identification of swirling flow in 3d vector fields. *Proc. AIAA Computational Fluid Dynamics Conference*, 95–1715.

Taira, K., Hemati, M. S., Brunton, S. L., Sun, Y., Duraisamy, K., Bagheri, S., Dawson, S. T. M., & Yeh, C.-W. (2017). Modal analysis of fluid flows: An overview. *AIAA Journal*, *55*(12), 4013–4041. https://doi.org/10.2514/1.J056060

Towne, A., Schmidt, O. T., & Colonius, T. (2018). Spectral proper orthogonal decomposition and its relationship to dynamic mode decomposition and resolvent analysis. *Journal of Fluid Mechanics*, *847*, 821–867. https://doi.org/10.1017/jfm.2018.283

Tryggvason, G., Scardovelli, R., & Zaleski, S. (2011). *Direct numerical simulations of multiphase flows*. Cambridge University Press. https://doi.org/10.1017/CBO9780511975264

Wang, Z., Zhang, G., Huang, H., Xu, H., & Sun, T. (2023). Joint proper orthogonal decomposition: A novel perspective for feature extraction from multivariate cavitation flow fields. *Ocean Engineering*, *288*, 116003. https://doi.org/10.1016/j.oceaneng.2023.116003

Xu, J., Dong, M., Zhou, J., Liang, Y., & Lu, J. (2024). Fast reconstruction of physical fields via pod and conditional deep convolutional gans. *International Journal of Green Energy*. https://doi.org/10.1080/15435075.2024.2322950

Yeo, H., & Lee, S. (2010). Stability of gas–liquid two-phase flows. *International Journal of Multiphase Flow*, *36*(6), 482–491. https://doi.org/10.1016/j.ijmultiphaseflow.2010.02.007

Zhang, Y., et al. (2023). Forecasting through deep learning and modal decomposition in two-phase concentric jets. *Expert Systems with Applications*, *232*, 120817. https://doi.org/10.1016/j.eswa.2023.120817